Chalcogenide Letters Vol. 20, No. 8, August 2023, p. 549- 558

Annealing effect on the photocurrent response of SnS thin films prepared by the chemical spray pyrolysis method

D. Dekhil [a *], H. Guessas [a], A. Nouri [a], S. Ullah [b]
[a] *Laboratory of Photonics Systems and Nonlinear Optics, Institute of Optics and Precision Mechanics, University Setif 1, Algeria*
[b] *Design and Manufacturing Institute (IDF)-Polytechnic University of Valencia (UPV), Valencia, Spain*

SnS thin films were synthesized using the spray pyrolysis method and then annealed at 350, 400, and 450°C. According to the crystallographic analysis, the obtained SnS thin films crystallized in the polycrystalline orthorhombic system. The grains measured 47, 66, and 37 nm for the samples annealed at 350, 400, and 450°C, respectively. SEM and AFM images indicate that the samples' surfaces were completely covered. Thus, the grains of SnS nanostructures have a granular-like shape and vary in size depending on the annealing temperatures. The transmittance measurement shows that annealing the sample at 400 °C extends and improves its absorption range to 600 nm. The resulting band gap energies were 1.60 eV, 1.30 eV, and 2.55 eV for annealing at 350 °C, 400 °C, and 450 °C, respectively. Hall Effect measurements reveal that annealing SnS films at 400 °C enhances their electrical properties. The values of carrier mobility, conductivity, and carrier concentration are 1.678 $\times 10^{5}$Cm2/Vs, 9.756 $\times 10^{-5}\Omega^{-1}cm^{-1}$, and 3.168 $\times 10^{10}Cm^{-3}$, respectively. Additionally, the photocurrent response validates that all samples annealed at 350, 400, and 450 °C have p-type conductivity, with values of 13, 28, and 2.5 µA/Cm2, respectively. The best conductivity, carrier mobility, and photocurrent values are obtained by annealing at 400 °C. Therefore, SnS thin films can be an interesting choice for absorber layer applications in photovoltaic systems.

(Received May 12, 2023; Accepted August 1, 2023)

Keywords: SnS, Thin films, Solar cell, Absorption, Photocurrent, conductivity

1. Introduction

Scientists have been working to develop solar cells with high conversion efficiency in response to the growing demand for renewable energy. Several materials with high conversion efficiencies have been commercialized in this context, including Gallium Arsenide (GaAs), Indium Phosphide (InP), monocrystalline silicon (c-Si) wafers, and cadmium telluride (CdTe). Because of the steep price increases for indium and gallium and the toxicity of cadmium and arsenide, the search for low-cost, readily available, and environmentally friendly photovoltaic materials has become critical [1]. Tin monosulfide (SnS) is one such material that is attracting the attention of researchers. The orthorhombic unit cell of SnS distinguishes it as a group IV-VI semiconductor material. This compound's bandgap energy is close to 1.3 eV, making it ideal for photovoltaic cells. With a theoretical conversion efficiency of 22%, a high absorption coefficient (> 10^{5} cm^{-1}), a hole concentration of 1018 cm^{-3}, and intrinsic p-type conductivity, SnS is also a promising material for photovoltaic conversion [2].

SnS thin films are synthesized using various chemical and physical techniques, including Sol-Gel, sputtering, electrodeposition, thermal evaporation, and ultrasonic spray coating [3]. These deposition techniques, followed by the annealing process, directly impact the material's properties and performance [4]. The most important structural characteristics affected by the annealing process are grain size and plan orientation, which affect both electrical properties and photocurrent

* Corresponding author: ahak2009@univ-setif.dz
https://doi.org/10.15251/CL.2023.208.549

response [5]. Several studies have shown that annealing SnS thin films change their photocurrent response significantly. The (111) plane becomes the preferred orientation after vacuum annealing an SnS film at 400 °C, with carrier concentration and mobility values of 10^{17} cm^{-3} and 18.06 cm^2 V^{-1} s^{-1}, respectively, according to Abadi et al. [4]. This yields a photocurrent response value of 20 $\mu A/Cm^2$.

Balakarthikeyan et al. [6] also demonstrate the effect of annealing (200-350 °C) on the photocurrent of nanostructured SnS films. According to the study's findings, the sample with the highest photocurrent value of 22 $\mu A/Cm^2$, attributed to improved crystalline structure and higher absorption, was annealed at 300 °C. Patel et al. [7] demonstrate how annealing SnS thin films deposited by spray pyrolysis at 500 °C can cause them to grow in the (111) direction and improve photocurrent response. Spray pyrolysis is one of the simplest methods because it is inexpensive, does not require vacuuming, and can be applied to large deposit surfaces. This method can be scaled up in the industrial sector [8]. The effects of annealing on the optical and electrical properties of SnS thin films synthesized by spray pyrolysis on ITO substrates are investigated in this study. Optimizing the photocurrent response of nanostructured SnS films by undergoing annealing is also investigated.

2. Experimental technique

SnS thin films were sprayed onto ITO-coated glass substrates using the spray pyrolysis technique. The aqueous solution was made by dissolving 100 mM tin (II) chloride ($SnCl_2$-$_2H_2O$, Sigma Aldrich) and 100 mM thiourea (CH_4N_2S, Sigma Aldrich) in two separate beakers, each with 100 ml of distilled water, for 15 min. The solution precursors were blended for 1 h at room temperature while constantly stirring. The remaining experimental conditions are held constant: sprayed volume (9 ml), flow rate (2 ml/min), compressed air (0.5 bar), hot plate temperature (100 °C), and nozzle-substrate distance (15 Cm). Finally, the obtained samples were thermally annealed for 60 min in the vacuum furnace at 350, 400, and 450 °C to improve crystalline quality.

Prior to each deposition, the glass substrate was thoroughly cleaned. In that order, the substrates were cleaned in an ultrasonic bath for 15 min in ethanol, acetone, and distilled water. The structural features of nanostructured SnS films were investigated using an X-ray diffractometer (PANalytical, Cu-kα = 1.5406). An AFM microscope was used to examine the surface topography. An SEM microscope equipped with an EDX spectrometer was used to scan surface images and determine elemental composition. The optical properties were determined using a UV-VIS spectrophotometer (Shimadzu UV-1800). The electrical properties were evaluated using Hall Effect and photocurrent measurements.

3. Results and discussions

3.1. Structural study

The structural properties of nanostructured SnS thin films were identified using the X-ray diffraction (XRD) technique, and the patterns are shown in Fig. 1. The orthorhombic SnS planes (0 2 1), (1 0 1), (1 1 1), (1 3 1), and (1 4 1) correspond to the strong diffraction peaks that appear at 26.24°, 30.50°, 31.50°, 39.04°, and 44.77°, respectively, according to JCPDS card No. 75-2115. Furthermore, no secondary phases were detected, confirming the purity of the SnS films' nanostructures [9]. The preferred orientation shifts from the (101) plane to the (111) plane as the annealing temperature rises from 350°C to 400°C [4]. According to Kang et al. [10], the change in preferential orientation caused by increasing annealing temperature suggests that the b-axis of the SnS unit cell is arranged perpendicular to the film's surface.

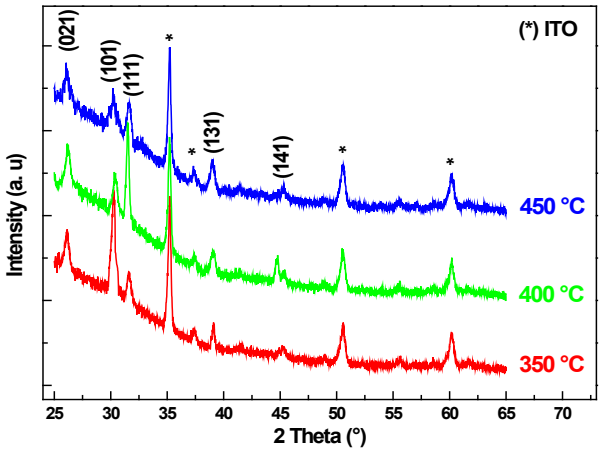

Fig. 1. X-ray diffraction patterns of SnS thin films annealed at 350,400, and 450 °C.

Furthermore, this b-axis configuration reduces the likelihood of interlayer shunt pathway formation. The SnS film unit cell parameters are calculated using the following relationship [11]:

$$\frac{1}{d_{hkl}^2} = \frac{h^2}{a^2} + \frac{k^2}{b^2} + \frac{l^2}{c^2} \tag{1}$$

where, (*h k l*) are Miller plane indices and *d* is the interplanar distance.

The average grain size of SnS thin films was calculated using the Deye-Scherrer equation [12] from the (111) XRD peaks:

$$D = \frac{0.9\lambda}{\beta \cos\theta} \tag{2}$$

where, θ denotes the Bragg angle of the (1 1 1) peak, β refers to the full width at half maximum (FWHM), and λ is the wavelength of the X-ray used (1.54 A°).

Table 1. Lattice parameters and grain size of nanostructured SnS thin films.

Annealing temperatures	(111) peak Position (°)	Parameters lattice (A°)				
		a	*b*	*c*	*FWHM (°)*	*D (nm)*
350 °C	31,60	4.330	11.189	3.986	0,35140	47
400 °C	31.50	4.321	11.190	3.981	0,24844	66
450 °C	31,60	4.327	11.210	3.879	0,44299	37

Table 1 summarizes the grain size and lattice parameter values of SnS nanostructures crystallized in the orthorhombic phase. The findings are comparable to those reported by Basak et al. [9]. The samples' lattice parameter values after annealing at 350 and 450 °C show that the cell contracts along the axis (*a, c*). The sample annealed at 400 °C has lattice parameters similar to those in JCPDS card No. 75-2115, indicating that the unit cell is not subject to contraction. The annealing process allows for 47, 66, and 37 nm grain sizes at 350, 400, and 450 °C, respectively (Table 1). Notably, when the annealing temperature reaches 450 °C, the grain size shrinks dramatically. This finding implies that annealing SnS thin films at temperatures above 400 °C may result in lattice degradation. This finding is consistent with the study by Javed et al. [13]. As a

result of these findings, annealing directly affects grain size, influencing optical and electrical properties.

3.2. Surface morphology

The surface morphology of nanostructured SnS thin films examined using an SEM microscope is depicted in Fig. 2(a-c). The films are highly nanostructured and have a smooth, crack-free surface with uniform-sized grains and high-quality crystallite. The surface annealed at 350 °C with more uniform-sized grains (around 120 nm) is shown in Fig. 2a. Furthermore, the grain distributions on the surface contain some randomly located voids. The measured grain size increases significantly (about 250 nm) as the annealing temperature rises from 350 °C to 400 °C.

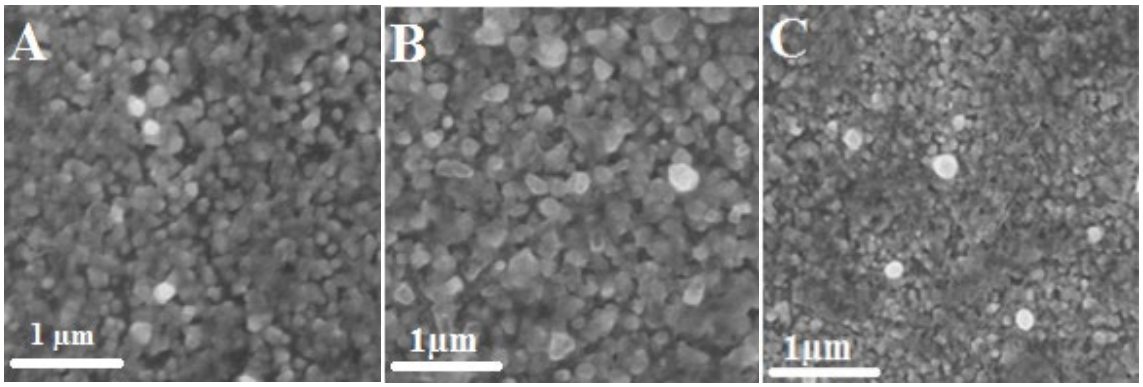

Fig. 2. SEM image of SnS thin films annealed at (a) 350 °C, (b) 400 °C, (c) 450 °C.

The voids then disappear, and the film becomes denser, resulting in large grains (Fig. 2b). Ahmed et al. [14] and Devarajan et al. [15] found similar results, stating that as the annealing temperature increased, grain size increased. Furthermore, as the annealing temperature increased to 450 °C, more voids appeared on the film's surface. As a result, these films are denser than those annealed at lower temperatures (Fig. 2.c). As a result of the high-temperature annealing, the grains lost their uniformity and shrank dramatically, causing SnS and Sn to uproot from the ITO substrate's surface. This result is consistent with the findings of Therno et al. [16].

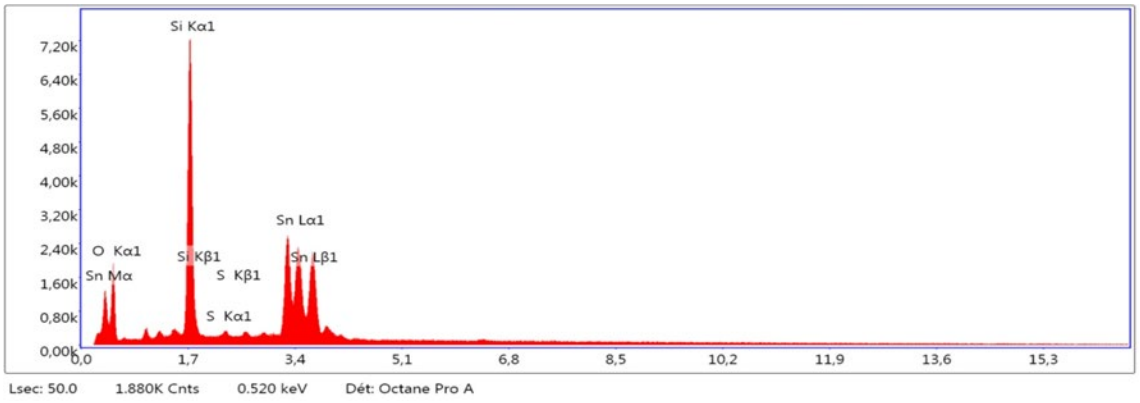

Fig. 3. EDX spectrum of SnS thin film annealed at 400 °C for 1 h.

Table 2. Composition of SnS thin films sprayed and annealed at 350, 400, and 450 °C obtained from EDX analysis.

Annealing temperature	Sn (at %)	S (at%)	Sn / S
350 °C	52.23	47.77	1.09
400 °C	50.53	49.47	1.02
450 °C	57.43	42.57	1.35

The qualitative and quantitative composition of nanostructured SnS films is determined using Energy Dispersive Spectroscopy (EDX). The EDX analysis of the films annealed at 400 °C, like the other films, is shown in Fig. 3. It demonstrated the presence of fundamental SnS film components (tin and sulfur), as shown in Fig 3. Other elements (such as Si and O) can also be found in EDX spectra, owing to the substrate in which they are present [17]; on the other hand, annealing at 350-400 °C results in better stoichiometry (Table 2). A slight excess of Sn was undoubtedly evaporated from the substrate during annealing at 450 °C [18]. The non-stoichiometry of nanostructured SnS films annealed at 450 °C is caused by two factors. The first could be caused by excess tin atoms and/or Sn+2 vacancies, resulting in deep acceptor states with activation energies ranging from 0.22 to 0.45 eV [18]. Excess tin atoms evaporate from the ITO-coated glass substrate during the second, higher-temperature annealing and are incorporated into SnS films. Sulfur deficiency is also caused by the S element evaporating from SnS films.

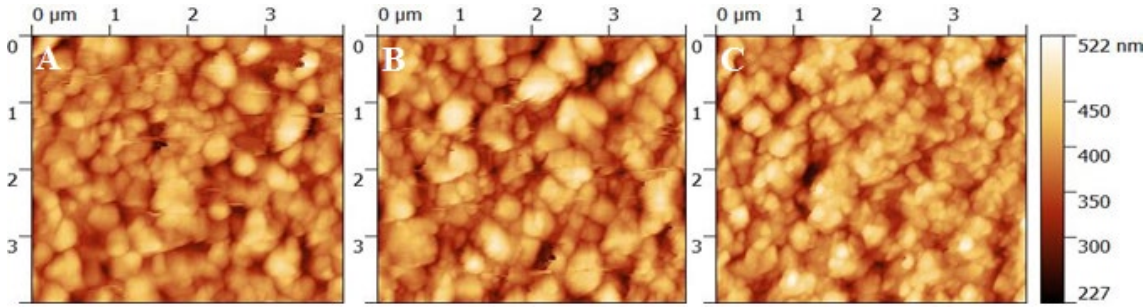

Fig. 4. 2D AFM images of SnS thin films annealed at (A) 350 °C, (B) 400 °C and (C) 450 °C.

Fig. 4 shows topography 2D images (4x4 μm^2) of nanostructured SnS films scanned by an AFM microscope. (a-c). SnS films are dense and evenly distributed across all sample surfaces, as shown in Fig 4. The thin films also have a granular morphology with homogeneous grain. These findings are consistent with those reported by Javed et al. [13]. In addition, the surface morphology change identifies the effect of annealing on nanostructured SnS films. Fig. 4a shows the surface after annealing at 350 degrees Celsius. Small granules of uniform size and shape agglomerated to form larger ones. The granules condense into larger grains when the temperature is raised to 400 degrees Celsius. As a result, grain boundary density decreases, resulting in denser SnS films (Fig. 4b). In contrast, annealing at a higher temperature (450 °C) causes granules to split and some voids to appear, resulting in a surface that appears porous. Indeed, annealing temperature, like grain size, directly influences roughness. In this case, AFM image analysis revealed that the RMS roughness was 38 nm, 59 nm, and 23 nm, respectively, corresponding to annealing at 350, 400, and 450 °C. The AFM analysis and RMS agree with the XRD results and are consistent with the literature [13, 17].

3.3. Optical studies

Fig. 5 depicts the transmission spectra of sprayed nanostructured SnS films on an ITO-coated glass substrate. Because the resulting SnS films have high visible absorption, they are better suited for use as absorber thin films in photovoltaic cells [19]. As shown in Fig. 5, as the annealing temperature was increased from 350°C to 400°C, the absorption range improved and expanded to

600 nm. This improvement in absorption is due to increased grain size. This correlation can be explained by more photon recombination on the preferential (111) plan, which has fewer grain boundaries and weak light scattering [10,20]. It can also be noted that higher-temperature annealing (450 °C) reduced the absorption range to 500 nm. This is due primarily to surface voids and a reduction in grain size. The literature [5] strongly supports this finding.

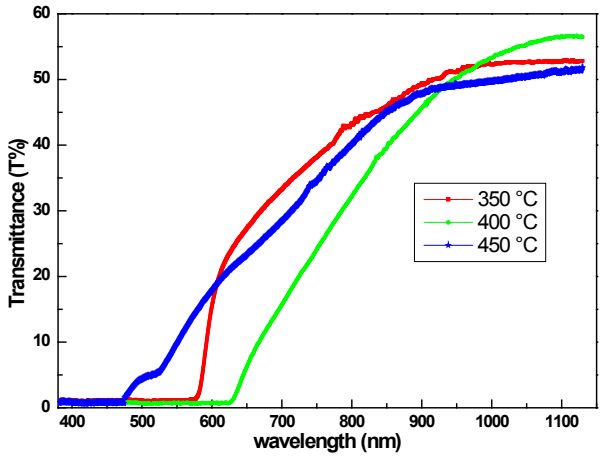

Fig. 5. Transmittance spectra of SnS thin films annealed at 350, 400, and 450 °C.

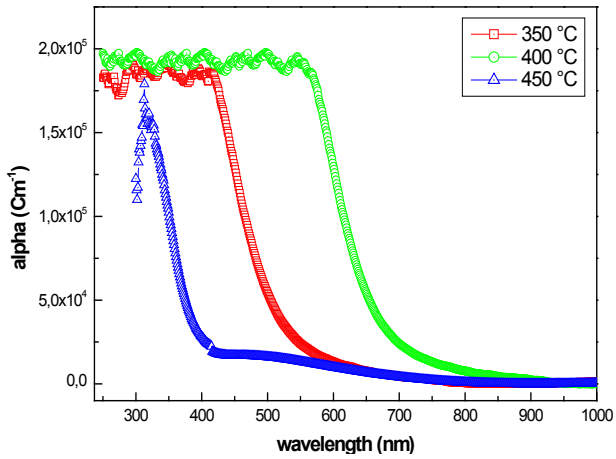

Fig. 6. The absorption coefficient of SnS thin films annealed at 350, 400, and 450 °C.

The plot of the absorption coefficients of nanostructured SnS films versus wavelength is shown in Fig. 6. As expected, higher absorption coefficients (>10^5 Cm^{-1}) were obtained for the annealing temperatures of 350 and 400 °C and as a result of improved grain compaction, the annealing at 400 °C yielded the highest absorption coefficient (22 x 10^5 cm^{-1}). It improves optical properties and increases light absorption in compact and dense materials [19]. The absorption edge was significantly shifted, as shown in Fig.5, indicating that the annealing temperature strongly influences the band gap E_g. A Tauc plot derived from the expression below [21] was used to calculate the optical band gap E_g.

$$(\alpha h\nu)^2 = A[h\nu\text{-}E_g] \tag{3}$$

where, *v and h* are the frequency of light and the Planck constant, respectively, and *A* is a constant that varies depending on the transition.

Fig. 7 shows a graph of $(\alpha hv)^2$ versus photon energy (hv). The optical band gap is determined by extrapolating the linear portion of these curves to the energy axes. The resulting E_g energy of nanostructured SnS films is 1.60, 1.30, and 2.55 eV, as shown in Fig. 7. The sample annealed at 400 °C has a lower optical band gap energy (1.30 eV), which is comparable to photovoltaic materials [22]. According to XRD patterns and Hall Effect measurements, this band gap shrinkage could be attributed to grain size enhancement and increased carrier concentration. This result demonstrates that SnS thin films absorb visible light effectively and are more suitable for use as thin absorber layers in photovoltaic cells.

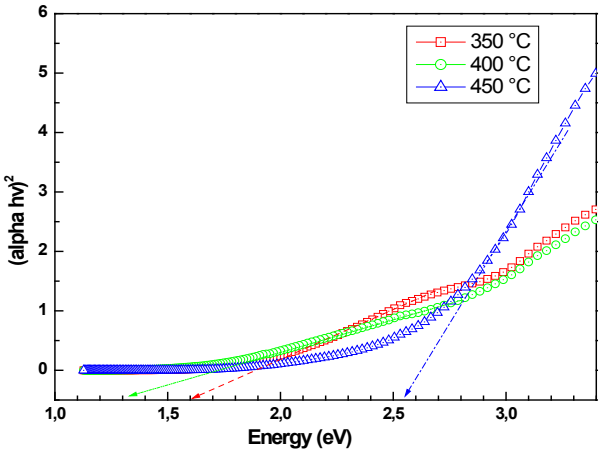

Fig. 7. Plots of $(\alpha hv)^2$ vs. hv of SnS thin films annealed at 350, 400, and 450 °C.

3.4. Electrical studies

The electrical properties of nanostructured SnS films, such as carrier mobility, conductivity, and Hall coefficient, were measured using the Hall Effect (Table 3). The results show that the Hall coefficients for each sample are positive, indicating that the intrinsic conductivity of the SnS films obtained is naturally p-type. Furthermore, the electrical properties vary due to the annealing, indicating that this annealing significantly impacts these properties (Table 3). Annealing at 400 °C produces better electrical properties than annealing at 350 °C. Whereas annealing at 450 °C reduces these properties and causes SnS film performance to deteriorate.

Table 3. Electrical parameters of SnS thin films annealed at 350, 400, and 450 °C.

Annealing Temperature (°C)	Carrier mobility (cm^2/Vs)	Conductivity $(\Omega cm)^{-1}$	Resistivity (Ωcm)	Carrier concentration (cm^{-3})	Hall coefficient $R_H(cm^3/c)$
350	7.579×10^4	4.698×10^{-5}	3.543×10^4	9.150×10^9	0.895×10^{10}
400	1.678×10^5	9.756×10^{-5}	1.433×10^4	3.168×10^{10}	1.927×10^{10}
450	6.786×10^4	8.921×10^{-6}	2.121×10^4	2.137×10^{10}	1.073×10^{10}

Furthermore, increasing the annealing temperature from 350°C to 400°C increases the carrier concentration and mobility from 9.150×10^9 (cm^{-3}) and 7.579×10^4 (cm^2/Vs) to 3.168×10^{10} (cm^{-3}) and 1.678×10^5 (cm^2/Vs), respectively. This improvement could be attributed to improved crystallization and increased grain size in the films, which could improve grain boundary reduction, crystal bonding reduction, and crystal defect reduction, allowing electrons trapped at the grain boundary to be released. Following that, the conductivity of the film increases while its resistivity decreases. Reduced carrier concentration and mobility (22.137×10^{10} cm^{-3}, 6.786×10^4 cm^2/Vs) were observed in films annealed at 450 °C. This finding means that annealing above 400

°C causes crystallization to fail in the SnS lattice. Their semiconducting properties suffer as a result. This decrease could be attributed to defects in the SnS lattice caused by higher-temperature annealing, accompanied by tin atom release. As a result, these defects act as dispersion centers, increasing the resistivity of the films. These findings are consistent with those reported by Daniel et al. [23].

At 0.5 volts for 120 seconds, the photoconductivity of nanostructured SnS films was investigated. The samples were sequentially exposed to multiple on-off (10 s) cycles of light radiation. The cathodic current density generated by the nanostructured SnS films reveals the intrinsic conductivity of p-type once more (Fig. 8). This result validates the Hall Effect measurement and is supported by the literature [24]. Thus, annealing at 400 °C generates a significantly higher photocurrent (28 μA/cm^2) than annealing at 350 °C (13 μA/Cm^2). This increase in photocurrent value is primarily due to an increase in grain size with orientation along the (111) plane and a decrease in the grain boundary, increasing diffusion length. At the Fermi level, the (111) orientation is known to have a higher density of states, which can result in increased carrier concentration and mobility. This can increase charge carrier collection efficiency and, as a result, photocurrent response. These results are consistent with those of Devarajan et al. [25].

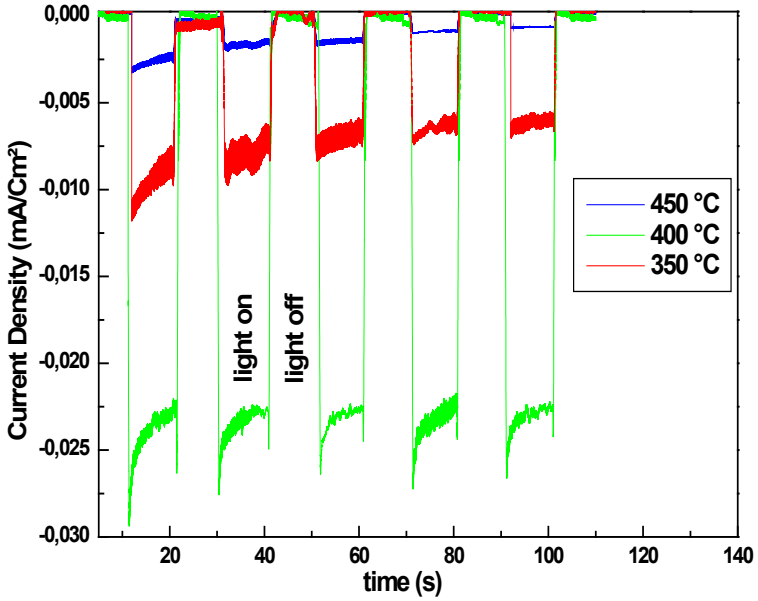

Fig. 8. Photocurrent response of the SnS thin films annealed at 350, 400, and 450 °C.

Moreover, this increase in photocurrent could be explained as follows: when the sample is illuminated, the generation of charge carriers results in some recombining with corresponding opposite charges. The barrier potential at the grain boundaries was reduced due to this process. This decrease facilitates carrier movement across boundaries, increasing charge carrier mobility [20]. Furthermore, the sample annealed at 450 °C shows a significant regression in current density (near zero). This sharp decrease could be caused by grain fragmentation, which is accompanied by the breaking of the SnS lattice's conduction mechanism caused by the uprooting of tin atoms from the surface of the films.

Stability and response time were also used to assess the photoreactivity of SnS films. The sample, annealed at 400°C, exhibits strong stability over time at the same intensity throughout all illumination cycles, as shown in Fig. 8 [24]. It can be noted that annealing at 350 and 450°C decreases photocurrent over time [26]. The passage of the OFF-ON cycle yields the second parameter, the response time (Fig. 8). As can be seen, films annealed at 350, 400, and 450 °C have response times of 0.65, 0.45, and 0.85 ms, respectively. In comparison to the response time (2.4 s) reported by Devarajan et al. [25,26], annealing SnS films at 400°C results in a much shorter

response time (0.45 ms). These findings imply that when annealed at 400 °C, SnS thin films have better stability and faster response times.

4. Conclusion

This study used spray pyrolysis to deposit SnS thin films on ITO-coated glass substrates heated to 100 °C. After that, the samples were annealed at 350, 400, and 450 °C. The XRD analysis revealed that the SnS films, which have a high-quality pure polycrystalline phase, crystallize primarily in the orthorhombic unit cell. The samples were annealed at 350, 400, and 450 °C, resulting in 47, 66, and 37 nm grain sizes, respectively. Images from SEM and AFM show that the grains are distributed uniformly and have surface voids. According to the optical study based on the transmittance spectrum, the SnS films annealed at 400°C have the best absorption span in the visible region, extending to 600 nm. Thus, the samples' annealing process contributes to band gap energies of 1.60, 1.30, and 2.55 eV, respectively. Furthermore, the films annealed at 350 and 400 degrees Celsius had a high absorption coefficient for visible light, greater than 10^5 Cm^{-1}. The intrinsic conductivity of p-type nanostructured SnS films is determined using Hall Effect measurements and confirmed by the photocurrent response.

Furthermore, annealing nanostructured SnS films at 400°C results in the best semiconducting properties, including photocurrent, which reaches 28 $\mu A/Cm^2$. This is due to larger grain sizes, which result in low density at the grain boundary, preventing charge recombination. As a result of the removal of potential barriers, charge mobility increased. Finally, annealing at 400 °C after aqueous solution-based synthesis of nanostructured SnS thin films improves optical and electrical properties, particularly photocurrent response. These findings show that SnS thin films are a superior candidate for use as thin absorber layers in photovoltaic cells.

References

[1] S.S. Hegde, A.G. Kunjomana, P. Murahari, B.K. Prasad, K. Ramesh, Surfaces and Interfaces 10, 78 (2018) ; https://doi.org/10.1016/j.surfin.2017.12.003

[2] T. Garmim, S. Chahib, L. Soussi, R. Mghaiouini, Z. El Jouad, A. Louardi, O. Karzazi, M. El Jouad, E. K. Hlil, B. Hartiti, M. Monkade, J Mater Sci: Mater Electron 31, 20730 (2020) ; https://doi.org/10.1007/s10854-020-04586-y

[3] J. A. Andrade-Arvizu, M. C. Piedrahita, O. Vigil-Galan, J Mater Sci: Mater Electron 26, 4541 (2015) ; https://doi.org/10.1007/s10854-015-3050-z

[4] A. Abadi, M. T. Htay, Y. Hashimoto, K. Ito, N. Momose, Japanese Journal of Applied Physics 61, SB1042 (2022) ; https://doi.org/10.35848/1347-4065/ac3a8f

[5] H. Choi, N. Lee, H. Park, Yeonsik. Choi, K. Kim, Yeongtae. Choi, J. Kim, S. Song, H. Yuk, H. Jeon, Appl. Sci 9(21), 4606 (2019) ; https://doi.org/10.3390/app9214606

[6] R. Balakarthikeyan, A. Santhanam, A. Khan, A. M. El-Toni, A. A. Ansari, A. Imran, M. Shkir, S. AlFaify, Optik 244, 167460 (2021) ; https://doi.org/10.1016/j.ijleo.2021.167460

[7] M. Patel, I. Mukhopadhyay, A. Ray, Optical Materials 35, 1693 (2013) ; https://doi.org/10.1016/j.optmat.2013.04.034

[8] S. R. Castro, J. N. Ríos, G. Escalante, G. Santana, A. S. Juárez, C. Á. Macías, IEEE 7th (WCPEC), 3305 (2018)

[9] A. Basak, A. Hati, A. Mondal, U. P. Singh, S.K. Taheruddin, Thin Solid Films 645, 97 (2018) ; https://doi.org/10.1016/j.tsf.2017.10.039

[10] J. Kang, S. Kwon, S. H. Yang, J. Cha, J. A. Bae, C. Jeon, Journal of Alloys and Compounds 711, 294 (2017) ; https://doi.org/10.1016/j.jallcom.2017.04.001

[11] E. Guneri, F. Gode, C. Ulutas, F. Kirmizigul, G. Altindemir, C. Gumus, Chalcogenide Letters 7, 685 (2010)

[12] N. Anitha, M. Anitha, L. Amalraj, Optik 148, 28 (2017) ;

https://doi.org/10.1016/j.ijleo.2017.08.139
[13] A. Javed, N. Khan, S. Bashir, M. Ahmad, M. Bashir, Materials Chemistry and Physics 246, 122831 (2020) ; https://doi.org/10.1016/j.matchemphys.2020.122831
[14] N. M. Ahmed, F. A. Sabah, H.I. Abdulgafour, A. Alsadig, A. Sulieman, M. Alkhoaryef, Results in Physics 13, 102159 (2019) ; https://doi.org/10.1016/j.rinp.2019.102159
[15] D. Alagarasan, S. S. Hegde, S. Varadharajaperumal, K. D. Arun Kumar, R. Naik, S. P. Panjalingam, E. S. Massoud, R. Ganesan, J Mater Sci: Mater Electron 33, 4794 (2022) ; https://doi.org/10.1007/s10854-021-07668-7
[16] T. Sall, B. M. Soucase, M. Mollar, J. Angel Sans, Journal of Electronic Materials 46, 1714 (2017) ; https://doi.org/10.1007/s11664-016-5215-9
[17] S. Sebastian, I. Kulandaisamy, A. M. S. Arulanantham, S. Valanarasu, A. Kathalingam, A. Jesu Jebathew, M. Shkir, M. Karunakaran, Optical and Quantum Electronics 51, 100 (2019) ; https://doi.org/10.1007/s11082-019-1812-1
[18] T. Sall, M. Mollar, B. M. Soucase, J Mater Sci 51, 7607 (2016) ; https://doi.org/10.1007/s10853-016-0039-9
[19] R. Essajai, A. El Hat, H. Shaili, W. Battal, E. Salmani, N. Hassanain, A. Mzerd, Materials Research Innovations, 1(2020)
[20] Y. Gupta, P. Arun, Physica Status Solidi (b) 253(3), 509 (2015) ; https://doi.org/10.1002/pssb.201552249
[21] J. Soudi, K.M. Sandeep, B.K. Sarojini, P.S. Patil, S.R. Maidur, K.M. Balakrishna, Optik 225, 165835 (2020) ; https://doi.org/10.1016/j.ijleo.2020.165835
[22] E. Guneri, C. Ulutas, F. Kirmizigul, G. Altindemir, F. Gode, C. Gumus, Applied Surface Science 257, 1189 (2010) ; https://doi.org/10.1016/j.apsusc.2010.07.104
[23] T. O. Daniel, U. E. Uno, K. U. Isah, U. Ahmadu, Revista Mexicana de Física 67 (2), 263 (2021) ; https://doi.org/10.31349/RevMexFis.67.263
[24] S. Ullah, A. Bouich, H. Ullah, B. Mari, M. Mollar, Solar Energy 204, 654 (2020) ; https://doi.org/10.1016/j.solener.2020.04.095
[25] D. Alagarasan, S. S. Hegde, S. Varadharajaperumal, R. Aadhavan, R. Naik, M. Shkir, H. Algarni, R. Ganesan, Phys. Scr 97, 065814 (2022) ; https://doi.org/10.1088/1402-4896/ac6d19
[26] D. Alagarasan, S. Varadharajaperumal, K. D. Arun Kumar, R. Naik, S. Umrao, M. Shkir, S. AlFaify, R. Ganesan, Optical Materials 121, 111489 (2021) ; https://doi.org/10.1016/j.optmat.2021.111489